Robotic Assisted MRI-Guided Interventional Interstitial MR-Guided Focused Ultrasound Ablation in a Swine Model

Jacquelyn MacDonell, MS[*]
Niravkumar Patel, PhD[‡]
Gregory Fischer, PhD[‡]
E. Clif Burdette, PhD[§]
Jiang Qian, MD PhD[¶]
Vaibhav Chumbalkar, MBBS[¶]
Goutam Ghoshal, PhD[§]
Tamas Heffter, MSc[§]
Emery Williams, BS[§]
Matthew Gounis, PhD[‖]
Robert King, PhD[‖]
Juliette Thibodeau[*]
Gene Bogdanov, PhD[‖]
Olivia W. Brooks, BS[#]
Erin Langan, BS[#]
Roy Hwang, MD[*]
Julie G. Pilitsis, MD PhD[*,**]

[*]Department of Neurosurgery, Albany Medical College, Albany, New York; [‡]Department of Mechanical Engineering, Worcester Polytechnic Institute, Worcester, Massachusetts; [§]Acoustic MedSystems Inc, Savoy, Illinois; [¶]Department of Pathology, Albany Medical College, Albany, New York; [‖]Department of Radiology, University of Massachusetts Medical School, Worcester, Massachusetts; [#]Department of Radiology, New England Center for Stroke Research, University of Massachusetts Medical School, Worcester, Massachusetts; [**]Department of Neuroscience and Experimental Therapeutics, Albany Medical College, Albany, New York

Correspondence:
Julie G. Pilitsis MD, PhD,
Department Neuroscience and Experimental Therapeutics,
Department of Neurosurgery,
47 New Scotland Ave, MC 10,
Albany, NY 12208.
E-mail: jpilitsis@yahoo.com

Received, October 18, 2017.
Accepted, May 21, 2018.
Published Online, June 14, 2018.

BACKGROUND: Ablative lesions are current treatments for epilepsy and brain tumors. Interstitial magnetic resonance (MR) guided focused ultrasound (iMRgFUS) may be an alternate ablation technique which limits thermal tissue charring as compared to laser therapy (LITT) and can produce larger ablation patterns nearer the surface than transcranial MR guided focused ultrasound (tcMRgFUS).

OBJECTIVE: To describe our experience with interstitial focused ultrasound (iFUS) ablations in swine, using MR-guided robotically assisted (MRgRA) delivery.

METHODS: In an initial 3 animals, we optimized the workflow of the robot in the MR suite and made modifications to the robotic arm to allow range of motion. Then, 6 farm pigs (4 acute, 2 survival) underwent 7 iMRgFUS ablations using MRgRA. We altered dosing to explore differences between thermal dosing in brain as compared to other tissues. Imaging was compared to gross examination.

RESULTS: Our work culminated in adjustments to the MRgRA, iMRgFUS probes, and dosing, culminating in 2 survival surgeries; swine had ablations with no neurological sequelae at 2 wk postprocedure. Immediately following iMRgFUS therapy, diffusion-weighted imaging, and T1 weighted MR were accurate reflections of the ablation volume. T2 and fluid-attenuated inversion-recovery (FLAIR) images were accurate reflections of ablation volume 1-wk postprocedure.

CONCLUSION: We successfully performed MRgRA iFUS ablation in swine and found intra-operative and postoperative imaging to correlate with histological examination. These data are useful to validate our system and to guide imaging follow-up for thermal ablation lesions in brain tissue from our therapy, tcMRgFUS, and LITT.

KEY WORDS: Brain tumor, High intensity focused ultrasound, Interstitial focused ultrasound, MRI-Guided, Neural ablation, Robot assisted surgery

Neurosurgery 84:1138–1148, 2019 DOI:10.1093/neuros/nyy266 www.neurosurgery-online.com

Ablative therapies have become increasingly used in the treatment of epilepsy, movement disorders, and brain tumors. Current therapies include transcranial magnetic resonance (MR) guided focused ultrasound (tcMRgFUS) and laser interstitial thermal therapy (LITT). Both have limitations in the size of the lesion that can be produced as large target volumes increase the risk of overheating the skull with tcMRgFUS and carbonization of tissue adjacent to LITT probes creates a gradient effect that limits laser penetration.[1,2] Further, tcMRgFUS cannot be used accurately near the skull because of the relative echogenicity. Here, we propose interstitial MR guided focused ultrasound (iMRgFUS) as an alternative ablative technique using sonic waves to create an area of thermal energy that destroys the target tissue. iMRgFUS is invasive and is inserted through a cannula similar to LITT. Our cannula also

ABBREVIATIONS: **DWI,** diffusion-weighted imaging; **FFE,** fast field echo; **FLAIR,** fluid-attenuated inversion-recovery; **H&E,** Hematoxylin and Eosin; **iFUS,** interstitial focused ultrasound; **iMRgFUS,** interstitial MR guided focused ultrasound; **LITT,** laser interstitial thermal therapy; **MR,** magnetic resonance; **MRgRA,** MR-guided robotically assisted; **MRTI,** MR thermal imaging; **SWI,** Susceptibility weighted imaging; **tcMRgFUS,** transcranial magnetic resonance (MR) guided focused ultrasound; **TTC,** triphenyltetrazolium-chloride

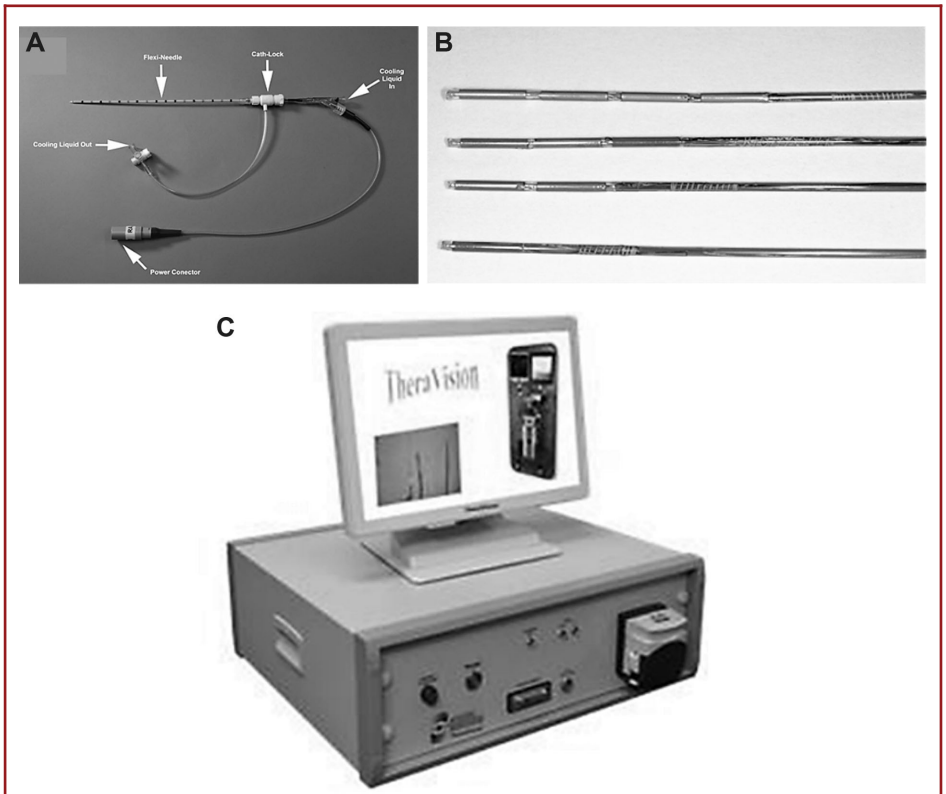

FIGURE 1. **A**, *Photo of an applicator inserted into a catheter used for the experiment.* **B**, *Fabricated ultrasound applicators with 1, 2, 3, and 4 transducers.* **C**, *TheraVision™ ultrasound thermal therapy system (Acoustic Medsystems) with 1 to 4 RF output channels used to power each transducer element.*

allows for concurrent biopsy of the lesion. iMRgFUS, similar to LITT, requires guidance with magnetic resonance imaging thermometry (MR thermal imaging [MRTI]). Previous work has been published using interstitial therapeutic ultrasound ablation technology.[3-5] However, here we discuss a complete system and workflow for delivery of thermal therapy using robotic placement under MR image guidance coupled with interstitial therapeutic ultrasound monitored by MRTI.

The workflow of MR guided neurosurgical procedures has been challenging.[6] To streamline the procedure in the MR, we developed an MRI-guided robotic assistant (MRgRA) to deliver iMRgFUS.[6-17] Specifically, this robotic assistant has 7 degrees of freedom and is constructed with a structure that moves similarly to a stereotactic frame. However, it is automated and capable of transitioning into alignment concurrently with imaging being obtained. In this study, we describe our work towards validating a complete set of tools for real time MRgRA delivery of interstitial focused ultrasound (iFUS) in a swine model. We present postmortem sections from post-iMRgFUS swine and imaging at various time points after thermal ablation. We correlate diffusion weighted, T1 with and without gadolinium, T2, susceptibility weighted, and fluid-attenuated inversion-recovery (FLAIR) imaging sequences with actual lesion size.

METHODS

Swine Model

All procedures were reviewed and approved by the Institution of Animal Care and Use Committee. Swine were approximately 10 wk old weighing between 30 and 40 kg. In an initial 3 animals, we optimized the workflow of the robot in the MR suite, and made modifications to the robotic arm to allow range of motion to reach the right and left frontal lobe and the cannula to penetrate the brain.[18] We optimized the use of Slicer software (3D Slicer, http://www.slicer.org) for neuronavigation use.[19] Accuracy during these experiments mirrored our phantom experience which showed a root mean square error 1.38 ± 0.45 mm in tip position and 2.03 ± 0.58° in insertion angle.[6]

In the next 4 swine, we worked to optimize the MR sequences obtained, the dose, and the duration. In this group, susscrofa domestica swine were sacrificed immediately following iMRgFUS treatment. The third subset of swine (n = 2) were evaluated for a 2-wk period following iMRgFUS treatment and then sacrificed. A total of 7 ablations in the

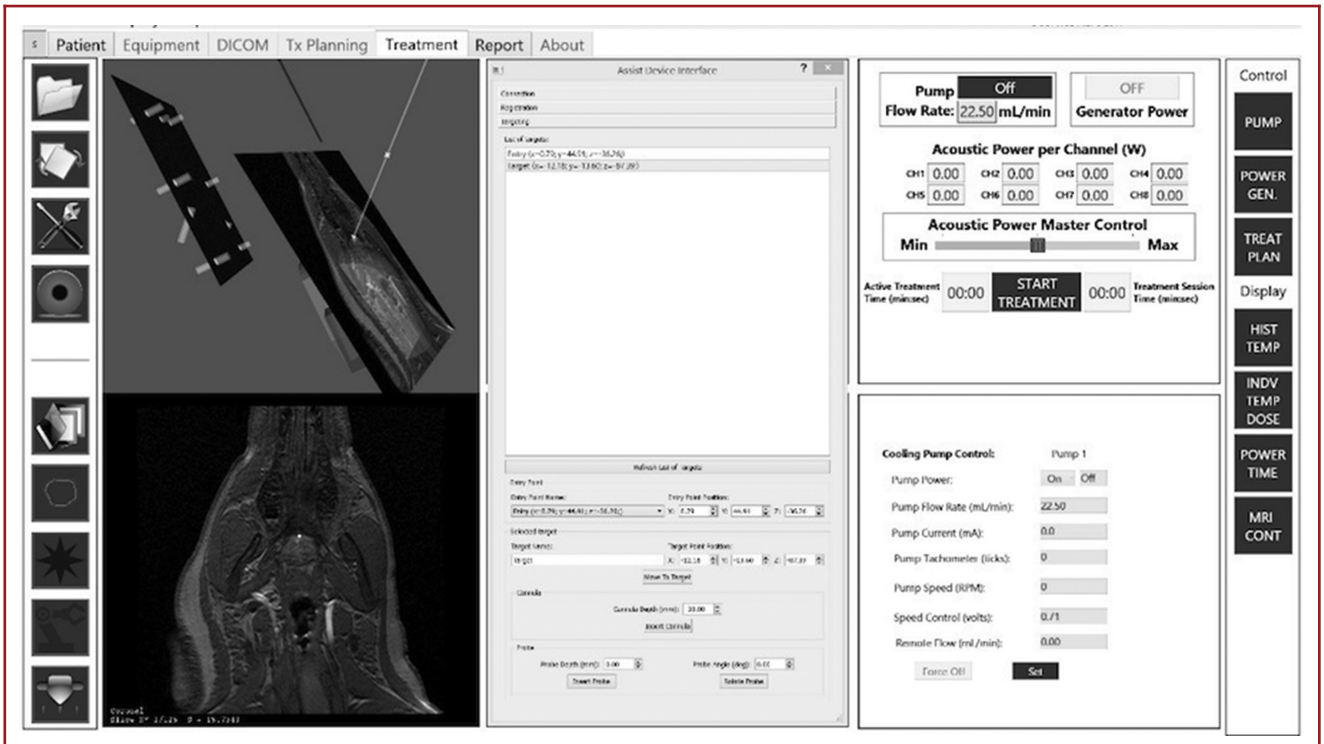

FIGURE 2. *Registration of the robot using multiple coronal images of the fiducial frame (top left image). By attaching the fiducial frame to the robot and then acquiring a stack of coronal images, the registration transformation from the image coordinate system and the robot coordinate system is determined using software algorithms developed during this program.*

second and third cohorts (n = 6) with MR imaging were performed with 1 receiving bilateral therapy. In all procedures, general anesthesia was induced and animals were carefully monitored. Preoperative doses of levetiractem (30 mg/kg) and dexamethasone (0.5 mg/kg) were used in survival surgeries.

The incision and burr hole was made near Kocher's point, and adjusted based on the target site. One-centimeter (cm) burr holes were made using a high-speed drill. The dura was opened, and a small corticectomy made. Sterile gelatin with gadolinium was placed in the incision to prevent cerebrospinal fluid egress and allow for localization. The wound was then closed. The animal was then moved into the MR, iMRgFUS therapy performed (documented in clinical workflow section), and postprocedure MRI obtained. Swine in acute surgeries were euthanized following iMRgFUS with a lethal dose of sodium pentobarbital and bilateral common carotid artery perfusion was performed using heparin and 4% paraformaldehyde.

The survival group was observed for a 2-wk period following iMRgFUS. Animals received daily physical exams and weekly neurological exams. Motor function score ranged from 0 to 2 points with 0 being considered normal motor function. A score of 2 indicated that the animal was not able to keep its foot in a normal position.[20] Social scores involved observation of swine behavior and measurement of the physiological responses of the animals.[21] Swine were monitored for a 10-min period per neurological exam. Behavioral parameters included restlessness, agitation, aggression and isolation. Maximum score per observation was 7. At day 7 and day 14 postoperatively, the survival animals underwent MRI. Following the 2-wk evaluation, animals were euthanized following final MRI using a lethal dose of sodium pentobarbital.

iMRgFUS Ablation

Multielement high-frequency tubular piezoelectric transducers with a 360° insonation pattern mounted on a hollow polyimide tubular structure were used to deliver therapy (Figures 1A–1C; ACOUST$_x$ applicators [Acoustic Medsystems, Savoy, Illinois]). We needed to reduce the transducer from 10 mm to 7 mm length during the acute studies when we realized that energy was transmitting to the subarachnoid space leading to bleeding. Applicators were inserted into the tissue, using a 13-gauge implant catheter. Degassed water was circulated through the catheter for cooling and acoustic coupling. Transducer center frequency ranged from 6.5 to 7.5 MHz with acoustic efficiency greater than 80%. The lesions formed were spheroid corresponding to length of each active element with uniform cylindrical volume in the central region and curved at the tip of the end of the active elements. These applicators have not demonstrated decrease in efficiency or central frequency after used for more than 20 procedures.

Clinical Workflow of MRI-Guided Robot-Assisted Thermal Ablator

1. The robot was registered to the MRI scanner coordinate system with a fiducial frame attached to the platform, composed of 9 tubes filled

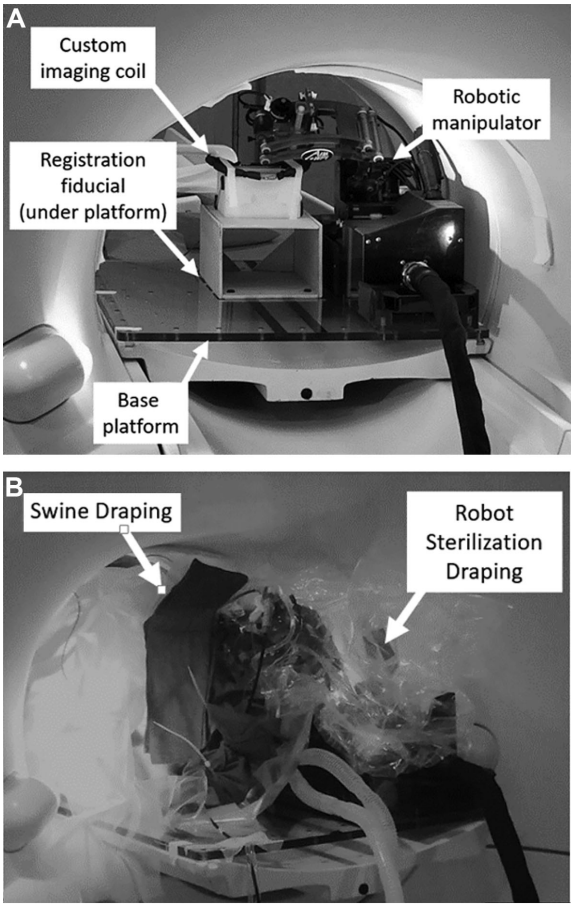

FIGURE 3. **A**, *Robotic manipulator and base platform without draping.* **B**, *Sterile environment for survival surgeries created by draping both the animal and robot manipulator in a sterile plastic sheet. Wires and tubing leaving the robot manipulator were wrapped in a sterile surgical cloth that was secured by zip ties.*

with MRI-visible, high contrast fluid and configured in a set of Z shapes similar to that of Eslami et al.[22] Localization of the robot with respect to the animal was accomplished by using multiple coronal images of the Z shaped framework (Figure 2).

2. Animals were then placed in the MR scanner upon the platform in prone position and their heads immobilized.
3. T1-Fast Field Echo (FFE) sequences were obtained and used to select the cannula entry point and target in Slicer. Locations were then transferred to and selected using labeled markers per the TheraVision system (Acoustic Medsystems), an imaging tool for our ultrasound ablation system.
4. A sterile environment was created for the scanner, animal and robot manipulator in survival cases (Figures 3A and 3B).
5. Using the defined entry and target locations, the robot aligned the cannula. After the incision was opened and gelatin removed, the cannula was inserted to a fixed depth stop and T1FFE sequences were taken to confirm the placement of the cannula.
6. After confirmation of cannula placement, the applicator was attached and the robot inserted the ablation probe through the cannula.
7. After the probe was inserted, confirmation MR images were acquired to affirm the probe location and orientation. The stack of 3 to 5 parallel image planes for MR-temperature monitoring were defined to be perpendicular to the probe's axis, centered at the transducer.
8. The net acoustic power doses were entered into TheraVision and the treatment was initiated and monitored in real time with MRTI (Table 1).
9. The ablator was retracted, the cannula removed, the robot commanded to move away from the surgical site, the incision closed, and postoperative MR images obtained (Figure 4).

MRI Sequencing

Acquisition was performed using a Philips Achieva 3-Tesla(3T) MRI scanner (Koninklijke Philips NV, MX Amsterdam, The Netherlands) equipped with a custom single-channel receive-only surface coil (Figure 5A). This 6 inch, 152 mm diameter coil is constructed primarily from 12 American wire gauge (AWG) 2.05 mm diameter copper wire. The capacitor breaks were reinforced with a pair of FR4 fiberglass boards on either side of the wire. The wire structure permits adjusting the coil geometry to conform to the load, or to clear obstacles (Figure 5b). It also occupies minimal space, which is a very significant issue near the robotic

TABLE 1. Thermal Ablation Dose Administration in Swine

	Experimental group	Acoustic output power (W)	Duration R frontal or temporal lobe (s)	Duration L frontal or temporal lobe (s)	Predicted ablation volume (cm^3)
Surgery 1	Acute	4	180	N/A	4.26
Surgery 2	Acute	4	180	120	L: 4.26; R: 2.21
Surgery 3	Acute	6	180	N/A	5.20
Surgery 4[a]	Acute	3	N/A	150	1.63
Surgery 5[a]	Survival	4[b]	120	N/A	–
Surgery 6[a]	Survival	3	100	N/A	0.44

[a]Used ablator probe with 7-mm element instead of 10-mm element.
[b]TheraVision software system became unresponsive during HIFU treatment and was manually shut off. Watts delivered during that time is unknown.

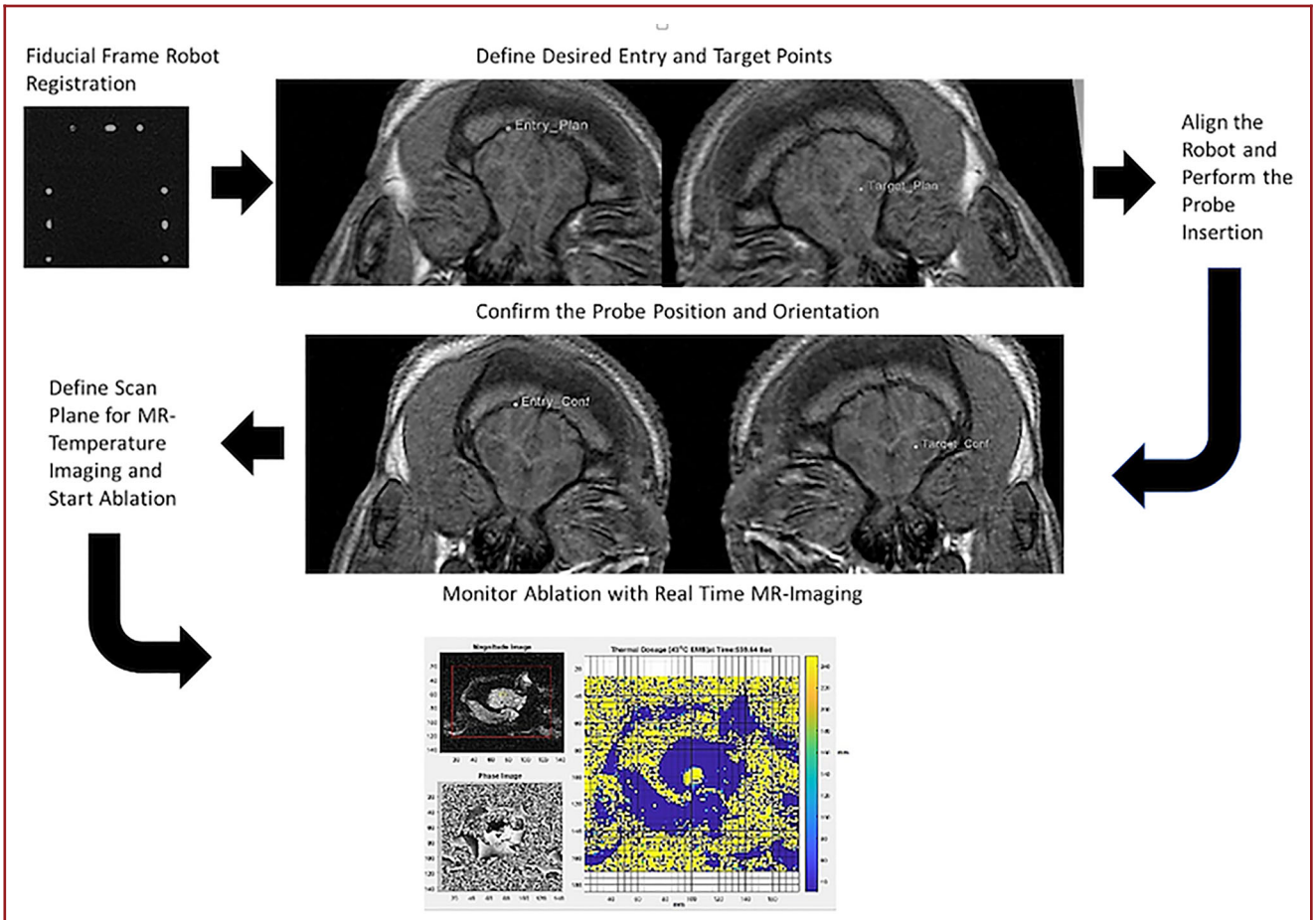

FIGURE 4. *MR images used throughout the procedure starting with fiducial frame robot registration (top left) and ending with MRTI (bottom).*

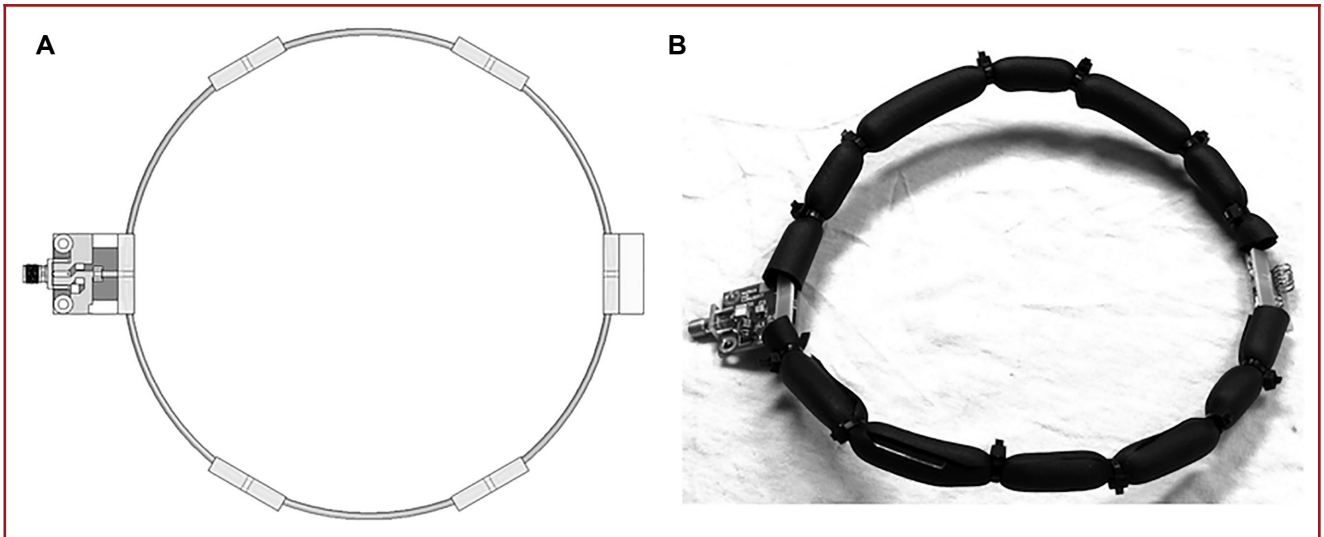

FIGURE 5. *Custom wire surface coil for pig brain imaging:* **A**, *CAD model;* **B**, *prototype with insulation and wires bent into the desired shape.*

arm. This coil's interface circuitry featured active and passive detuning. All images had FoV 150 mm, 2 mm slice thickness and matrix 150/150. T1W-SE imaging was done both precontrast, and 5 min postinjection of 0.2 mmol/kg gadopentetate (Magnevist, Bayer), with TR/TE 691/11, FA 70° NSA 2. T2W-TSE used a TR/TE of 9700/80, FA 90°, NSA 4, ETL 19. T2-FLAIR used a TR/TE 1100/125, TI 2800, FA 90°, NSA 3, ETL 27. Diffusion-weighted imaging used a modified TSE with TR/TE 3100/76, FA 90°, b-value 1000, direction 3, NSA 6, ETL 31. Susceptibility weighted imaging (SWI) used a modified T1W-FFE with TR/TE 26/18, gap −0.5 mm, FA 10°, NSA 1. For survival surgeries, postoperative MR-imaging sequences were taken at 3 time intervals: immediately following iMRgFUS therapy (tp0), 1-wk post-iMRgFUS therapy (tp1), and at 2-wk post-iMRgFUS therapy (tp2).

Histological Evaluation

In a subset of animals (n = 3), assessment of ablation zone was performed with triphenyltetrazolium-chloride (TTC) staining, based on previous methodology.[23] In the remaining cases (n = 3), sections were postfixed in 4% paraformaldehyde for 1 wk. Zivic Pig Brain Slicer (Zivic Instruments, Pittsburgh, Pennsylvania) was used to section blocks at 5 mm. Sections were stored in 1 molar phosphate-buffered saline with 30% sucrose at 3°C. Hematoxylin and Eosin (H&E) staining was performed in the ablation zone and surrounding region.

Ablation Volumes

Photographs of tissue with adjacent rulers were uploaded to ImageJ (NIH funded open access software, https://imagej.nih.gov/ij/). Pixels on the photograph were converted into units by selecting the straight-line tool, outlining 1 cm along the ruler and setting the scale to the known distance. The area and slice thickness were then used to determine the ablation volume in cm.[3] MRI ablation volumes were measured for each imaging sequence with DICOM Viewer (Koninklijke Philips NV) using the freehand tool. The area and slice thickness were used to determine the ablation volume. Volume measurements were taken twice by 2 individuals, p_1 and p_2, to account for variations in measurement techniques across individuals. Bland Altman analysis was used to quantify agreement between the two quantitative measurements by constructing the limits of agreement which are defined as the mean difference ± 1.96 standard deviation of difference.[24]

RESULTS

A total of 3 acute swine studies were performed to optimize workflow of the system. Specifically, modifications of the robotic arm to expand its reach to the contralateral frontal region and of our Slicer-based surgical planning system were needed. Imaging and pathology in our initial ablation cases revealed over time that the 10 mm iFUS device led to dispersion of energy into the subarachnoid space and a 7 mm iFUS device was subsequently designed (Figure 6). We began studies using an acoustic output power and treatment time extrapolated from work in the liver. It became clear that brain tissue responded differently, and subsequently duration and wattage was varied to determine a safe dosing pattern. Table 2 demonstrates predicted ablation volumes based on previous work in liver tissue as there was no predicate for brain tissue with iMRgFUS.

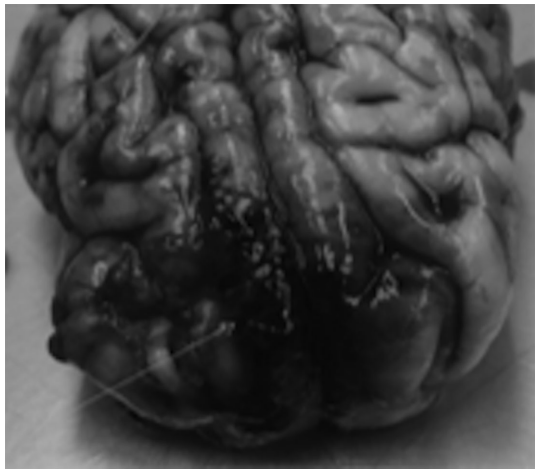

FIGURE 6. *Postexplant examination revealing subarachnoid blood.*

Lesions were created on both right and left frontal lobes, with target varying from superior, middle, and inferior frontal gyrus. At tp0, diffusion-weighted imaging (DWI) and T1 images were available for all animals, while SWI, T2, and FLAIR were only available for 2 animals (Table 3; Figure 7). DWI correlated with histological ablation zones with limits of agreement from −0.967 cm^3 to 0.540 cm^3. A total of 4 of 7 ablation zones were not visualized on T1 images with or without gadolinium. In the 3 cases where the ablation zone was visualized, measurements were similarly accurate to DWI (comparison to histological section with limits of agreement that ranged from −0.406 cm^3 to 0.853 cm^3). Ablation was not evident in the subset that underwent T2 and FLAIR sequences while SWI changes did not correlate with brain slices, limits of agreement from −6.27 cm^3 to 13.40 cm^3.

For the survival studies, DWI, SWI, T1, T2, and FLAIR were available in both animals at tp1 and tp2 (Table 2). In the first animal DWI, SWI, and T1 at all-time points showed the ablation zone. In the second animal, no changes were seen in tp1 and tp2 in DWI. All other sequences noted ablation. Only SWI and FLAIR showed changes at tp2. DWI for the first survival surgery was an accurate reflection of the ablation volume at both tp1 and tp2 with ablation volumes differing from histological measurements by −0.61 cm^3 and 0.095 cm^3, respectively. T2 imaging at tp1 was a more accurate representation of ablation volume when compared to T1 at tp1 for both survival surgeries with T1 and T2 limits of agreement ranging from −1.11 cm^3 to 0.76 cm^3 and −0.41 cm^3 to 0.45 cm^3, respectively. Although ablation at tp2 was only seen on 1 of the survival surgeries on T1 and T2, they were both accurate reflections of the ablation volume differing from histological section by −0.45 cm^3 and −0.194 cm^3, respectively. SWI became more accurate overtime but was least accurate of measures. FLAIR was the most accurate reflection of ablation

TABLE 2. Mean Ablation Volume

Mean ablation volume (cm^3)	DWI	SWI	T1[a]	T2	FLAIR	Histology	Predicted in vivo liver tissue
Surgery 5 tp0	0.17	n/a	x[a]	N/A	N/A		–
Surgery 5 tp1	0.49	1.28	0.61[a]	0.24	0.35		–
Surgery 5 tp2	0.23	0.91	0.55	0.29	0.36	0.10	–
Surgery 6 tp0	0.43	0.23	0.25[a]	x	x		0.44
Surgery 6 tp1	x	0.52	0.07[a]	0.06	0.2		0.44
Surgery 6 tp2	x	0.30	x[a]	x	0.09		0.44

N/A: MR-sequence not available; x: sequence did not demonstrate ablation.
[a]Indicates gadolinium.

TABLE 3. Ablation Volume

	DWI	SWI	T1[a]	T2	FLAIR	Histology	Predicted
Surgery 1 tp0	8.23 cm^3	1.49 cm^3	8.16	x	x	8.61 cm^3	4.46
R Surgery 2 tp0	1.41 cm^3	N/A	X	N/A	N/A	0.87 cm^3	4.16
L Surgery 2 tp0	2.35 cm^3	N/A	2.79[a]	N/A	N/A	1.52 cm^3	2.21
Surgery 3 tp0	0.31 cm^3	N/A	X	N/A	N/A	0.12 cm^3	5.20
Surgery 4 tp0	0.32 cm^3	N/A	X	N/A	N/A	0.27 cm^3	1.63
Surgery 5 tp0	0.17 cm^3	N/A	X	N/A	N/A	0.10 cm^3	–
Surgery 6 tp0	0.43 cm^3	0.23 cm^3	0.25[a]	x	x	0.24 cm^3	0.44

N/A: MR-sequence not available; x: sequence did not demonstrate ablation.
[a]Indicates gadolinium.

volume at tp2 with limits of agreement from −0.61 cm^3 to 0.02 cm^3.

Both animals had edema at tp1 on FLAIR imaging. At tp2, the first animal had residual, but considerably improved edema. The edema in animal 2 was completely resolved at tp2. Both animals had normal behavioral scores. Of note, animal 1 had difficulties emerging from anesthesia, which resolved when dexamethasone was administered. Additionally, 1 d postoperatively the animal care staff noted a seizure-like event where the animal became stiff-legged and fell on its side for 60 s. The animal recovered from the event without intervention. Within 4 h after ablation in an acute animal, the brain was extracted and fixed. After gross evaluation, H&E staining was performed (Figures 8A and 8B). In this animal, acoustic output was set to 6 W for 180 s and the probe was located in the right temporal lobe.

Intra- and Interobserver Variability

For the 2 volume measurements taken by p_1, the difference between volumes ranged from −0.118 cm^3 to 0.13 cm^3 with a mean difference of −0.0081 cm^3. Limits of agreement were determined to be −0.106 cm^3 to 0.09 cm^3. The limits of agreement for p_2 ranged from −0.171 cm^3 to 0.14 cm^3 with a mean difference of −0.0059. When the mean volume measured by p_1 was compared to the mean volume measured by p_2 the limits of agreement were determined to be 0.473 cm^3 to −0.579 cm^3 with a mean difference of 0.0529 cm^3.

DISCUSSION

Optimizing Robotic Delivery of iFUS

We successfully performed 7 iMRgFUS ablations (5 acute and 2 survival) on 6 swine, after optimizing robotic delivery of iFUS in an initial subset of animals (n = 3). Optimization included: (1) increasing robotic arm range of motion to the contralateral side, (2) decreasing the distance from the robotic arm to the skull to allow the cannula to penetrate into the brain, (3) customized probes to not affect subarachnoid space, and (4) dose response for brain where thermal energy needed is much lower than for other tissues.

MRI and Thermal Ablation

Imaging was available in the remaining 6 swine. Restricted diffusion on DWI and hyperintensity in T1 with gadolinium were accurate reflections of the ablation volume at tp0 and tp1. FLAIR was the most accurate reflection of ablation volume at tp2 and was additionally able to identify edema which was seen as a region of hyperintensity surrounding a central area of signal hypointensity

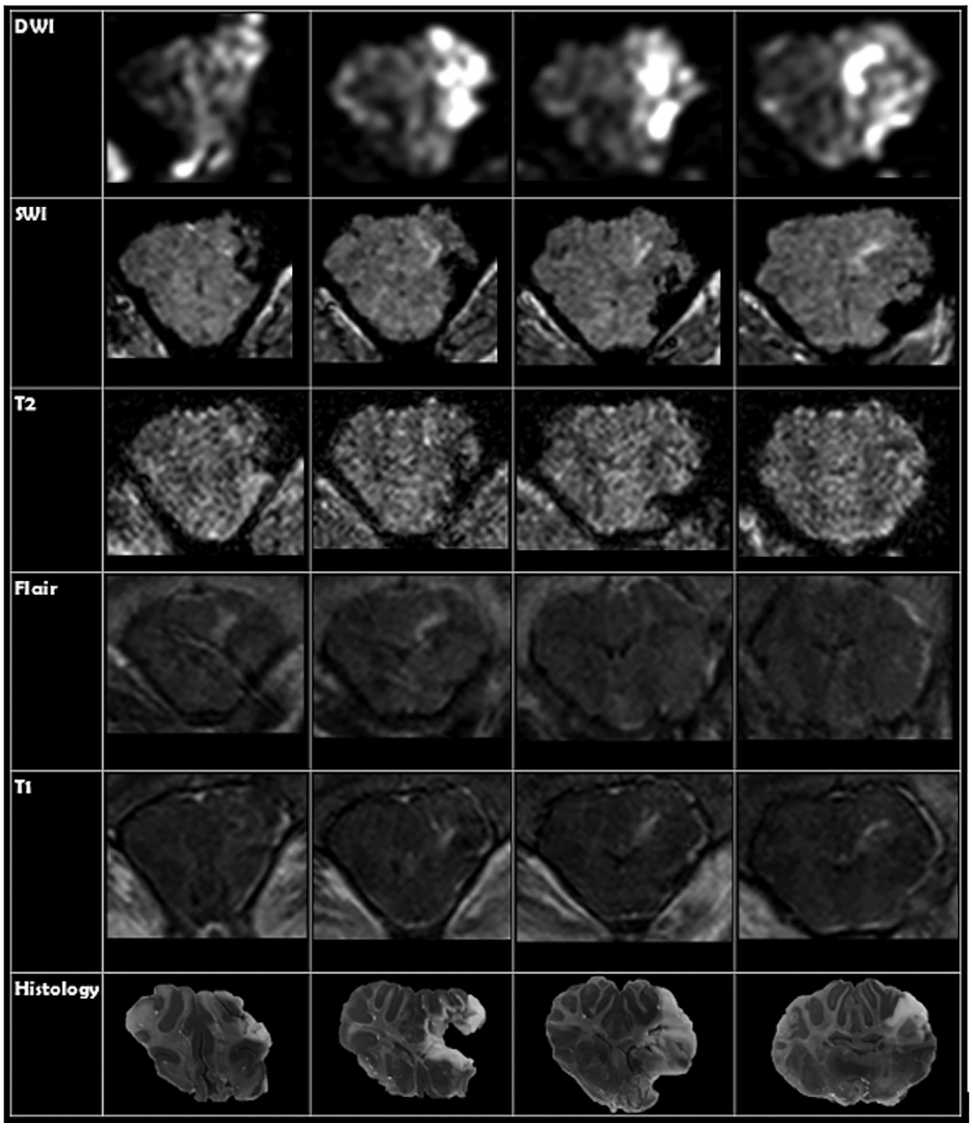

FIGURE 7. *Comparison of MRI imaging sequence to histological section for an acute surgery where TTC staining methods were utilized. Each row represents a different MR-imaging sequence taken at tp0. Each column represents an MRI slice taken at the same location as the histological section.*

that corresponded with ablation boundaries as seen on histology. From tp1 to tp2 much of the signal hyperintensity on both T2-weighted and FLAIR imaging dissipated, representing decreased edema.

Previous thermal ablation studies have used LITT therapy T2 and T1 pre- and postcontrast imaging to assess ablation zones.[12] Others have suggested role of ADC, another water diffusion measure like DWI.[25] Thermal ablation resulting from FUS can be thought of having 3 zones: the central zone, which is immediately radial from the interstitial ultrasound ablator and undergoes liquefactive necrosis, the transitional zone exposed to hyperthermia and surrounding tissue that is unaffected.[13] DWI may be visualizing a combination of that liquefactive necrosis as well as cell membrane disruption. Unfortunately, T1 and T2 sequences are known to have a slight delay in visualizing ablation volumes when compared to DWI, and it is already known that DWI can predict permanent injury faster than other sequences.[14] For simple volumes, this fact may not matter but when treating larger more complex volumes real-time evaluation of damaged tissue may be a necessity. DWI sequences in our data seem to correlate well with both early and late treatment effects when changes are apparent. Correlations of imaging and histology are

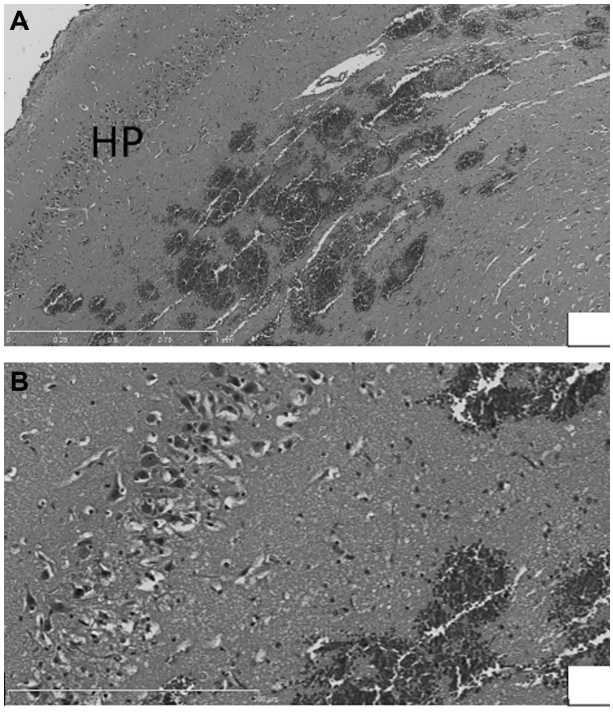

FIGURE 8. **A**, *Low power view (5×) of petechial hemorrhage in/near hippocampus.* **B**, *Higher power view (20×) of petechial hemorrhage in/near hippocampus, with edema and pyknotic and eosinophilic neurons visible (within rectangles).*

limited to animal models outside the brain. One showed a close correlation with T1 postcontrast imaging and histology 48 h postablation.[26]

Clinical Application

LITT, like iMRgFUS, utilizes thermal energy to ablate the target tissues. LITT procedures have been utilized for the treatment of epilepsy and brain tumors where ablation is delivered through a fiber optic applicator that must be inserted through a keyhole sized lesion in the skull.[27] MRTI is utilized throughout the treatment course to monitor the distribution of heat and minimize damage to surrounding tissue. As a result of these similarities, we used the LITT procedure as a model for our clinical workflow. Although the procedures of these therapies are very similar, there are some key differences in how the thermal energy is produced and consequently on how the target tissue responds to treatment. There is, however, no doubt that the application of FUS energy in a delivery method similar to LITT therapy will allow the ablation of more complex and superficial tumors and also aid in facilitating its use in epilepsy surgery; especially since LITT is currently being applied to epilepsy surgery.[28,29] LITT therapy however cannot be performed adjacent to major blood vessels or in highly vascular lesions.[2] Conversely, FUS appears to preferentially injury ganglion cells, glial cells, white matter, then blood vessels from greatest to in order of less vulnerable tissue.[30] Therefore, theoretically FUS may be safer in regard to vascular lesions and lesions close to vasculature.[9] Other advantages of our iMRgFUS device are its ability to target lesions close to the skull. FUS has already found use in thalamotomy for essential tremor, but other potential applications include treatment of brain tumors, pain and epilepsy,[30] especially with iMRgFUS technologies.

Limitations

Of note, while we showed appropriate correlation between postmortem brain sections and imaging, the predicted lesion size for postmortem sections generally did not correlate. This discrepancy is likely 2-fold. One is due to the fact that we predicted ablations based on our experience with liver; doses used for these brain ablations were generally proportional but different because of acoustic properties. Additionally, only single slice MRTI data were generally available. Unfortunately, this 2D MR thermometry accuracy is limited to only the temperature distribution information in that slice. In 3D MRTI, multiple slices are acquired in one plane and 3D reconstruction techniques are used to create a 3D image with higher spatial resolution and a higher signal to noise ratio allowing for more accurate volume calculations. Use of a preclinical navigation system also likely confounded the matter as even with 2D MRTI in humans there has been close correlation of MRTI with postoperative imaging at 1 d to 1 wk after surgery on T1 and T2 weighted imaging.[31] We will utilize a volumetric based MRTI and more sophisticated interface in the future.

CONCLUSION

We successfully performed 5 acute and 2 survival ablations using MRgRA for interstitial FUS delivery. Workflow improved during the course of experiments and dosing of iMRgFUS relative to brain was established. Probes and dosing were optimized. DWI was a reliable reflection of ablation volume immediately following therapy for all surgeries. Ablation volumes were demonstrated on FLAIR imaging in both survival animals at tp1 and tp2 and were accurate reflections of ablation volume. 3D MRTI is needed in future studies.

Disclosures

Dr Pilitsis is a consultant for Medtronic, Centauri, Boston Scientific, and Abbott and receives grant support from Medtronic, Boston Scientific, Abbott, Nevro, Jazz Pharmaceuticals, GE Global Research, and NIH 1R01CA166379. She is a medical advisor for Centauri and Karuna and has stock equity. Dr Burdette is the CEO of Acoustic MedSystems Inc and receives NIH support. Dr Ghoshal, Mr Heffter, and Mr Williams are all employees of Acoustic MedSystems Inc. Dr Gounis has been a consultant for Codman Neurovascular, InNeuroCo, Medtronic Neurovascular, and Stryker Neurovascular; holds stock in InNeuroCo; travel support from Neuravi; and has received research support from the NIH, Anaconda, CereVasc LLC, Codman Neurovascular, Gentuity, Microvention, Medtronic Neurovascular, Mivi Neuroscience, Neuravi, Philips Healthcare,

InNeuro, R92M, Rapid Medical, Stryker Neurovascular, the Stroke Project, and the Wyss institute. The other authors have no personal, financial, or institutional interest in any of the drugs, materials, or devices described in this article.

REFERENCES

1. McDannold N, Clement GT, Black P, Jolesz F, Hynynen K. Transcranial magnetic resonance imaging- guided focused ultrasound surgery of brain tumors. *Neurosurgery*. 2010;66(2):323-332; discussion 332.
2. Missios S, Bekelis K, Barnett GH. Renaissance of laser interstitial thermal ablation. *Neurosurg Focus*. 2015;38(3):E13.
3. Kangasniemi M, Diederich CJ, Price RE, et al. Multiplanar MR temperature-sensitive imaging of cerebral thermal treatment using interstitial ultrasound applicators in a canine model. *J Magn Reson Imaging*. 2002;16(5):522-531.
4. Herickhoff CD, Light ED, Bing KF, et al. Dual-mode intracranial catheter integrating 3D ultrasound imaging and hyperthermia for neuro-oncology: feasibility study. *Ultrason Imaging*. 2009;31(2):81-100.
5. Canney MS, Chavrier F, Tsysar S, Chapelon JY, Lafon C, Carpentier A. A multi-element interstitial ultrasound applicator for the thermal therapy of brain tumors. *J Acoust Soc Am*. 2013;134(2):1647-1655.
6. Li G, Su H, Cole GA, et al. Robotic system for MRI-guided stereotactic neurosurgery. *IEEE Trans Biomed Eng*. 2015;62(4):1077-1088.
7. Macdonell J, Patel N, Rubino S, et al. Magnetic resonance guided interstitial high-intensity focused ultrasound for brain tumor ablation. *Neurosurg Focus*. 2018;44(2):E11.
8. MacDonell J, Patel N, Rubino S, et al. Magnetic resonance-guided interstitial high-intensity focused ultrasound for brain tumor ablation. *Neurosurgical focus*. 2018;44(2):E11.
9. Youn Y, Walling IT, Gee L, et al. 353 High-intensity ultrasound for the treatment of vincristine-induced neuropathic pain. *Neurosurgery*. 2016;63(Suppl 1):204.
10. Wang Y, Cole GA, Su H, Pilitsis JG, Fischer GS. MRI compatibility evaluation of a piezoelectric actuator system for a neural interventional robot. *Conf Proc IEEE Eng Med Biol Soc*. 2009;2009:6072-6075.
11. Cole GA, Harrington K, Su H, Camilo A, Pilitsis JG, Fischer GS. Closed-loop actuated surgical system utilizing real-time in-situ MRI guidance. In: Khatib O, Kumar V, Sukhatme G, eds. *Experimental Robotics: The 12th International Symposium on Experimental Robotics*. Berlin, Heidelberg: Springer Berlin Heidelberg; 2014:785-798.
12. Cole GA, Pilitsis JG, Fischer GS. Design of a robotic system for MRI-guided deep brain stimulation electrode placement. *Paper Presented at: 2009 IEEE International Conference on Robotics and Automation*; May 12-17, 2009; Kobe, Japan.
13. Pilitsis JG, Cole GA, Fischer GS. Stereotaxy with Real-time MRI-guided Robot Assistance. *ASSFN*. Oral Presentation; San Francisco, CA; June 3-6; 2012.
14. Fischer GS, Burdette EC, Pilitsis JG. Development of MRI-guided robotic Hi-intensity ultrasound needle/catheter for ablation of brain. *Paper Presented at: CNS Annual Meeting*; Poster Presentation; Oct 18-20; 2014; Boston, Massachusetts.
15. Patel N, Li G, Bogdanov G, et al. Monitoring and control of iMRI-guided robot-assisted conformal brain tumor ablation. *11th Interventional MRI Symposium*; Abstract Presentation; Oct 7-8; 2016; Baltimore, MD.
16. Gee L, Burdette EC, Ghoshal G, et al. Interstitial directional high intensity focused ultrasound in a 6-hydroxydopamine lesioned rodent model of parkinson's disease. *Paper Presented at: AANS Annual Scientific Meeting*; Oral Presentation; April 30-May 4; 2016; Chicago, IL.
17. Ghoshal G, Gee L, Heffter T, et al. A minimally invasive catheter based ultrasound therapy for the brain. *Neurosurg Focus*. Accepted for publication Feb 2018;44(2):E13.
18. Nycz CJ, Gondokaryono R, Carvalho P, et al. Mechanical validation of an MRI compatible stereotactic neurosurgery robot in preparation for pre-clinical trials. *IEEE/RSJ International Conference on Intelligent Robots and Systems - IROS 2017*. Vancouver, BC, Canada; September 2017.
19. Norton I, Essayed W, Zhang F, et al. SlicerDMRI: open source diffusion MRI software for brain cancer research. *Cancer Res*. 2017;77(21):e101-e103.
20. Castel D, Sabbag I, Brenner O, Meilin S. Peripheral neuritis trauma in pigs: a neuropathic pain model. *J Pain*. 2016;17(1):36-49.
21. Reyes L, Tinworth KD, Li KM, Yau DF, Waters KA. Observer-blinded comparison of two nonopioid analgesics for postoperative pain in piglets. *Pharmacol Biochem Behav*. 2002;73(3):521-528.
22. Eslami S, Shang W, Li G, et al. In-bore prostate transperineal interventions with an MRI-guided parallel manipulator: system development and preliminary evaluation. *Int J Med Robot*. 2016;12(2):199-213.
23. Joshi CN, Jain SK, Murthy PS. An optimized triphenyltetrazolium chloride method for identification of cerebral infarcts. *Brain Res Protoc*. 2004;13(1):11-17.
24. Giavarina D. Understanding Bland Altman analysis. *Biochem Med*. 2015;25(2):141-151.
25. Hectors SJ, Jacobs I, Moonen CT, Strijkers GJ, Nicolay K. MRI methods for the evaluation of high intensity focused ultrasound tumor treatment: Current status and future needs. *Magn Reson Med*. 2016;75(1):302-317.
26. Fite BZ, Wong A, Liu Y, et al. Magnetic resonance imaging assessment of effective ablated volume following high intensity focused ultrasound. *PLoS One*. 2015;10(3):e0120037.
27. Tovar-Spinoza Z, Carter D, Ferrone D, Eksioglu Y, Huckins S. The use of MRI-guided laser-induced thermal ablation for epilepsy. *Childs Nerv Syst*. 2013;29(11):2089-2094.
28. Nowell M, Miserocchi A, McEvoy AW, Duncan JS. Advances in epilepsy surgery. *J Neurol Neurosurg Psychiatry*. 2014;85(11):1273-1279.
29. Jermakowicz WJ, Kanner AM, Sur S, et al. Laser thermal ablation for mesiotemporal epilepsy: Analysis of ablation volumes and trajectories. *Epilepsia*. 2017;58(5):801-810.
30. Christian E, Yu C, Apuzzo MLJ. Focused ultrasound: relevant history and prospects for the addition of mechanical energy to the neurosurgical armamentarium. *World Neurosurg*. 2014;82(3-4):354-365.
31. Elias WJ, Huss D, Voss T, et al. A pilot study of focused ultrasound thalamotomy for essential tremor. *N Engl J Med*. 2013;369(7):640-648.

Acknowledgment

Many thanks to Paul Feustel, PhD for his guidance in statistics.

COMMENTS

The authors created a pig model for testing a new method of high intensity focused ultrasound, now more commonly referred to as MR guided FUS. They demonstrate the technical feasibility of their method, in which a robot is used to insert cannulas for the delivery of ultrasonic energy, and also provide MRI and 1 histological image after the treatments. Small lesions with a sharp border were created where planned.

Of course, MRgFUS has been popularized so far as a way to make lesions in a narrow, central portion of the brain, such that thalamotomies for patients with essential tremor can be created. As such the technique is analogous to stereotactic radiosurgery, with heat and cavitation as the mechanism of action rather than ionizing radiation (and the capability of making reversible lesions). This is the 1 clinically proven and FDA-approved use of noninvasive MRgFUS to date. Instead, the authors invite us to think of MRgFUS in a way analogous to laser interstitial thermal therapy (LITT), which also uses heat as its method of energy. Their method allows MRgFUS to be applied anywhere within the brain, without the limitations imposed by an intact calvarium.

Time will tell if invasive MRgFUS will be superior to LITT in terms of lesion precision and the volumes it may be possible to treat. The authors are to be congratulated for rethinking this application and for testing it in a rigorous manner in vivo.

Michael Schulder
Manhasset, New York

In this study, the authors refined a platform to deliver interstitial high-intensity focused ultrasound to create lesions in the brains of healthy pigs, then evaluated MRI and histology after lesion creation to determine the imaging sequences that best correlate with histological findings after

thermal ablation. Six pigs underwent ultrasound ablation targeted using MRI thermography in the frontal or temporal lobes using a variety of ultrasound parameters. Six MRI sequences (T1 without contrast, T1 with contrast, T2, FLAIR, DWI, and SWI) were performed immediately after the procedure, and 2 of the animals underwent repeat imaging at 7 and 14 days. All animals were histologically examined to determine lesion size. The authors found that DWI and T1 correlated best with lesion size immediately after treatment, whereas T2 and FLAIR were most accurate at 1 week. They conclude that these results validate the system and also provide a framework for future imaging assessment of thermal ablation.

Interstitial ultrasound using multiple independently-powered transducers for tailored heating using real-time temperature-sensitive imaging is a potentially powerful method of stereotactic lesion generation that was proposed many years ago for treatment of intracranial lesions but has not yet entered clinical practice. The results of this study convincingly demonstrate that subjective assessment of postoperative imaging findings correlates with histological measurement of lesion size, which has important implications for further development of this technology. However, heterogeneity in the experimental design in this study makes it difficult to draw any conclusions about its accuracy: the intended lesion size was different in each animal; a different lesion duration, wattage, and probe type was used in every case; and the outcome measures (MRI sequences and histological assessment techniques) were not uniform. The authors were not able to produce the lesions they intended (actual lesion sizes were very different from what was predicted), which is unfortunate since the main advantage of this technology is the ability to produce precisely conformal lesions that can be controlled in real time. It is also unclear how characteristics of ablation of healthy tissue might be relevant to treatment of brain lesions that might respond differently. The use of interstitial ultrasound is a promising neurosurgical technique, but further work is necessary to establish its potential clinical utility.

Jonathan P. Miller
Cleveland, Ohio